

# UNCLASSIFIED

AD NUMBER
AD830445
NEW LIMITATION CHANGE
TO Approved for public release, distribution unlimited
FROM Distribution authorized to U.S. Gov't. agencies and their contractors; Administrative/Operational Use; Mar 1966. Other requests shall be referred to Air Force Flight Dynamics Lab [FDFR], Wright-Patterson AFB, OH 45433.
AUTHORITY
AFFDL ltr dtd 1 Feb 1973

THIS PAGE IS UNCLASSIFIED

AD 830445

AFFDL-TR 67-171

**MEASUREMENTS OF AVERAGE HEAT  
TRANSFER COEFFICIENTS FOR A MESH  
SIMULATING POROUS PARACHUTE CLOTH**

C. J. SCOTT  
E. R. G. ECKERT  
M. RUIZ-URBIETA

UNIVERSITY OF MINNESOTA

TECHNICAL REPORT AFFDL-TR-67-171

MARCH 1968

This document is subject to special export controls and each transmittal to foreign governments or foreign nationals may be made only with prior approval of the Air Force Flight Dynamics Laboratory.

*Attn: FDER W-P AFB, Ohio. 48433*

AIR FORCE FLIGHT DYNAMICS LABORATORY  
AIR FORCE SYSTEMS COMMAND  
WRIGHT-PATTERSON AIR FORCE BASE, OHIO

## NOTICE

When Government drawings, specifications, or other data are used for any purpose other than in connection with a definitely related Government procurement operation, the United States Government thereby incurs no responsibility nor any obligation whatsoever; and the fact that the Government may have formulated, furnished, or in any way supplied the said drawings, specifications, or other data, is not to be regarded by implication or otherwise as in any manner licensing the holder or any other person or corporation, or conveying any rights or permission to manufacture, use, or sell any patented invention that may in any way be related thereto.

This document is subject to special export controls and each transmittal to foreign governments or foreign nationals may be made only with prior approval of the AF Flight Dynamics Laboratory (FDFR) Wright-Patterson AFB, Ohio.

The distribution of this report is limited because the report contains technology identifiable with items on the strategic embargo lists excluded from export and re-export under U. S. Export Control Act of 1949 (63 Stat. 7) as amended (50 U.S.C. App. 2020.2031) as implemented by AFR 400-10.

Copies of this report should not be returned unless return is required by security considerations, contractual obligations, or notice on a specific document.

**MEASUREMENTS OF AVERAGE HEAT  
TRANSFER COEFFICIENTS FOR A MESH  
SIMULATING POROUS PARACHUTE CLOTH**

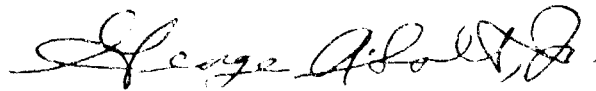
*C. J. SCOTT  
E. R. G. ECKERT  
M. RUIZ-URBIETA*

This document is subject to special export controls and each transmittal to foreign governments or foreign nationals may be made only with prior approval of the Air Force Flight Dynamics Laboratory.

## FOREWORD

This report summarizes the work done by the Heat Transfer Laboratory, Department of Mechanical Engineering, University of Minnesota, during a research program sponsored by the Recovery and Crew Station Branch of the Air Force Flight Dynamics Laboratory under Contract AF33615-67-1028, Project No. 6065, Task No. 606505. The manuscript was released by the authors November 1967 for publication as a Technical Report. The contract's technical project monitor was C. A. Babich III of the Air Force Flight Dynamics Laboratory (FDFR). E. R. G. Eckert served as principal investigator of the contract at the University of Minnesota. The report covers work conducted from August 1966 through September 1967.

This technical report has been reviewed and is approved.



GEORGE A. SOLT, JR.  
Chief, Recovery & Crew Station Branch  
Vehicle Equipment Division  
AF Flight Dynamics Laboratory

# ABSTRACT

Experimental heat transfer studies have been performed on three screens simulating a porous parachute. The average Nusselt number was measured as a function of the sonic Reynolds number. The range of the sonic Reynolds number extended from 5 to about 1400. Three different porosities and two different pressure ratios were used. Within the range of porosities and pressure ratios investigated, no significant effect of these parameters on the average heat transfer coefficient could be established. The Nusselt numbers for screens are shown to have a behavior quite similar to the Nusselt number for a single cylinder in cross flow. The relation  $Nu(L + D)/Re^* = 0.5$  appears to be an acceptable representation of the average Nusselt numbers on screens for sonic Reynolds numbers above 400 for which rarefaction effects are not present.

The distribution of this Abstract is unlimited.

## TABLE OF CONTENTS

Section	Page
I INTRODUCTION	1
II EXPERIMENTAL FACILITY	5
A. Low Density Wind Tunnel	6
B. Test Section	16
C. Instrumentation	19
III EXPERIMENTAL STUDIES	21
IV DISCUSSION OF RESULTS	29
V CONCLUSIONS	39
APPENDIX I. DATA REDUCTION TECHNIQUE	40
APPENDIX II. ESTIMATE OF CONDUCTION LOSSES	42
REFERENCES	44

## ILLUSTRATIONS

Figure	Page
1. Sketch of a Porous Parachute	2
2. Photograph of the Wind Tunnel	7
3. Sketch of Experimental Facility	8
4. Exploded View of Test Chamber	11
5. Aluminum Plate with Test Section and Housing Blocks	13
6. Aluminum Plate with Nozzle	14
7. One Test Screen	17
8. Example of Extrapolation Technique Used to Obtain $R_0$	24
9. $P_{up}/P_{down}$ versus $Re^*$ for Screen 1	26
10. $P_{up}/P_{down}$ versus $Re^*$ for Screen 2	27
11. $P_{up}/P_{down}$ versus $Re^*$ for Screen 3	28
12. Nusselt number versus $Re^*$ for Screen 1	30
13. Nusselt number versus $Re^*$ for Screen 2	31
14. Nusselt number versus $Re^*$ for Screen 3	32
15. Comparison of Present Results with Results for a Cylinder	33
16. $Nu/(Re^*)^{1/2}$ versus $Re^*$ for All Three Screens	37
17. Comparison of Experimental Results with Theoretical Prediction	39
18. Comparison of Experimental Results and the Results Corrected for Estimated Heat Conduction Losses	43



# SYMBOLS

A	convective heat transfer area (ft <sup>2</sup> )
a	speed of sound (ft/sec)
d	wire diameter (ft)
h	average convective heat transfer coefficient (BTU/hr-ft <sup>2</sup> -°F)
I	intensity of electrical current (amps)
k	thermal conductivity (BTU/hr-ft-°F)
Kn	Knudsen number
Ma	Mach number
Nu	Nusselt number, $= \frac{h_0}{k_0}$
P <sub>up</sub>	absolute total pressure upstream of the nozzle (mm of Hg)
P <sub>down</sub>	absolute static pressure downstream of test mesh (mm of Hg)
Po	geometric porosity
q	heat flux (BTU/hr-ft <sup>2</sup> )
R	electrical resistance of test mesh (ohms)
Re*	sonic Reynolds number, $= \frac{\rho^* a^* d}{\mu^*}$
Re <sub>1</sub>	Reynolds number, $= \frac{\rho_1 U_1 d}{\mu_1}$
T	temperature (°F)
u	velocity (ft/sec)
$\alpha$	temperature resistance coefficient (°F <sup>-1</sup> )
$\rho$	density (lbm/ft <sup>3</sup> )
$\mu$	viscosity (lb-sec/ft <sup>2</sup> )

### Superscripts

\* denotes sonic conditions, assuming isentropic expansion to sonic velocity

### Subscripts

aw denotes adiabatic wall conditions

f " flight conditions

0 " reference value

1 " conditions upstream of the grid

w " conditions of the screen's wires

## SECTION 1

### INTRODUCTION

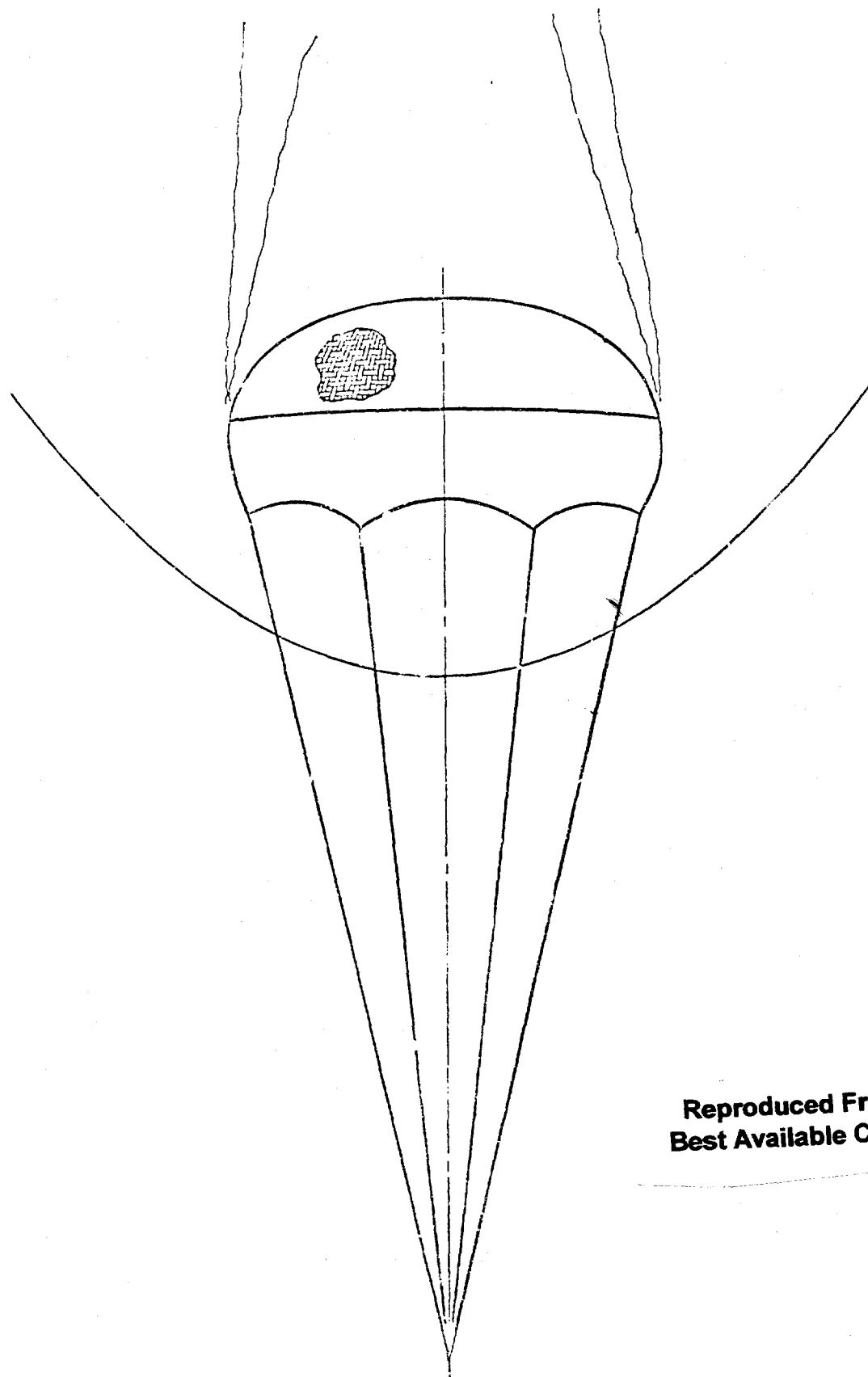
It is well known that by the aerodynamic heating effect, vehicles flying at supersonic speeds are heated to such an extent that the skin temperatures and the temperatures inside the craft require the special attention of the designer. In addition, a growing interest in aircraft vehicle recovery operations has directed attention to a variety of deceleration devices. In many cases a sizeable portion of the initial kinetic energy of the primary or forebody is converted into an increase in internal energy of the retardation device and the aerodynamic heat transfer of the deceleration device becomes a design factor.

Aerodynamic decelerators must possess a large drag-to-weight ratio and normally must be capable of being stored in a small volume. Therefore, most drag-producing devices are relatively thin and flexible. Towed decelerators such as ribbon or hyperflo parachutes, balloons, ballutes, etc., have flexible canopies. Other proposals incorporate structural members (cones or paragliders) or hybrid systems such as the AVCO drag brake (1)\* and the NASA rocornet (2).

Impermeable retardation devices are aerodynamically unstable when utilized in a supersonic flow. As a result, nearly all of the retardation devices discussed above employ extended porous surfaces in conjunction with venting techniques (see Figure 1). Most conventional textile fibers either melt or are seriously degraded by exposure to tempera-

---

\*Numbers enclosed by parentheses refer to references.



**Reproduced From  
Best Available Copy**

Figure 1. Sketch of a Porous Parachute

tures above 500°F. It is desirable to replace these fibers with materials of higher thermal durability such as fine metallic wires in which operational temperatures are close to 2000°F.

The flow field associated with a parachute results from the interaction of the large-scale phenomena enveloping the complete body and the small-scale processes associated with the local flow through a single porous element in the mesh material itself. The large-scale phenomena (parachute shape and size, velocity, altitude), which vary with the particular design, are generally involved with the aerodynamics of the problem and contribute end or boundary conditions (pressure ratio, Reynolds number) to the small-scale phenomena.

When opened at a flight Mach number exceeding unity, a parachute produces a bow shock immediately forward of the canopy. The flow impinging on the parachute material then is subsonic and normal to the surface except near the periphery of the canopy (3). Hence, for most of the surface area of the parachute an appropriate model is a woven mesh with the impinging flow normal to it. The flow is isentropically expanded to sonic conditions at the minimum area of the mesh, based on the open porosity of the canopy roof, and the flow then expands from the choked condition into supersonic jets bordered by free shear layers downstream (small-scale phenomena). Immediately behind the individual fibers a small region of recirculating, subsonic, vortex flow exists.

Heat will be transferred from the hot air to the screen. The heat transfer coefficient for a similar configuration is conventionally ex-

pressed by the following dimensionless relationship:

$$Nu = f(Re, Pr, Ma_f, Po) \quad (1)$$

Since a sonic throat condition occurs for supercritical pressure ratios, it appears of advantage to use a sonic Reynolds number defined as

$$Re_d^* = \frac{\rho^* a^* d}{\mu^*} \quad (2)$$

where the viscosity  $\mu^*$  is independent of the pressure  $p^*$  and a known function of the temperature  $T^*$ .

The Prandtl number  $Pr$ , whose value for air is approximately 0.7 under normal atmospheric conditions, deviates up to  $\pm 10$  percent from this value to temperatures of approximately 6000°R, from whereon the deviations become larger (4). A temperature of 6000°R corresponds to the stagnation conditions at  $Ma = 10$  and 50,000 feet altitude. At altitudes up to 400,000 feet the stagnation temperatures for  $Ma \leq 10$  will be below 6000°R. The deviation of the Prandtl number from the value 0.7 will be neglected in this report.

The flight Mach number  $Ma_f$  has only an indirect influence upon the heat transfer to the canopy because, in conjunction with the flight altitude, it will fix the stagnation pressure and temperature downstream of the shock. The Mach number appearing in the relation for the Nusselt number would have to be one indicating the flow conditions downstream from the wire grid because the upstream Mach number gives no information

on downstream conditions for a supercritical pressure ratio. It is then more straightforward to use the pressure ratio  $P_{up}/P_{down}$  in place of a Mach number.

The porosity<sup>\*</sup>  $P_o$  is used as a parameter describing the geometry of the wire screen.

The purpose of the experiments described in this report is to establish the relationship between the average Nusselt number, the Reynolds number  $Re_d^*$ , the pressure ratio  $P_{up}/P_{down}$ , and the porosity  $P_o$  for a fluid with a Prandtl number equal to 0.7.

---

<sup>\*</sup> Porosity is defined geometrically as the ratio of open area to total area of the forward-facing surface of the retardation device.

## SECTION II

### EXPERIMENTAL FACILITY

#### A. LOW DENSITY WIND TUNNEL

Figure 2 shows the experimental facility used. A small subsonic wind tunnel was constructed to simulate the flow rates and reduced pressures characteristic of the operation of supersonic parachutes. A small duct 2 inches in diameter, in which the flowmeter was located, was expanded into an 8-inch O.D. stilling chamber prior to flow through the test section. A mechanical vacuum pump-blower combination, with two interchangeable blowers, provided the necessary flow.

The open system is shown schematically in Figure 3. The system draws air from the laboratory room. It is composed of five components: air dryer, flow metering device, upstream and downstream valves, test chamber, and vacuum pump combination, each described in detail below.

##### 1. Air Dryer

The air dryer is an open-ended cylinder filled with calcium sulfide and one layer of glass wool. The dryer serves to dehumidify the incoming air below the limits specified for proper pump operation. It also provided a means of eliminating any condensation shocks that might occur. The calcium sulfide was changed daily during running periods to ensure optimum drying.

##### 2. Flow Metering Device

For the range of Reynolds numbers anticipated, three different metering devices were selected. Two sharp-edged flat-plate orifices,



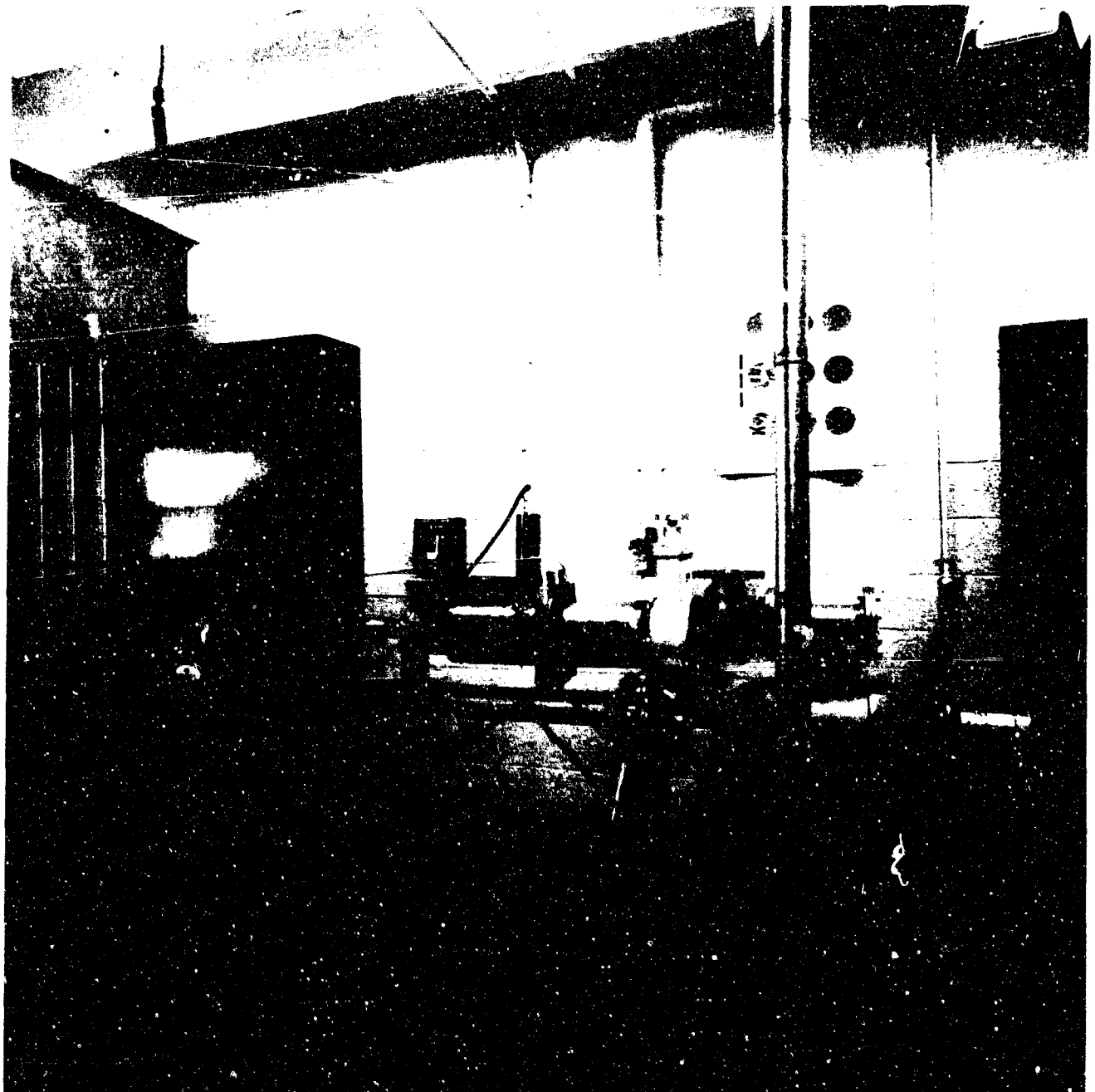


Figure 2. Photograph of the Wind Tunnel

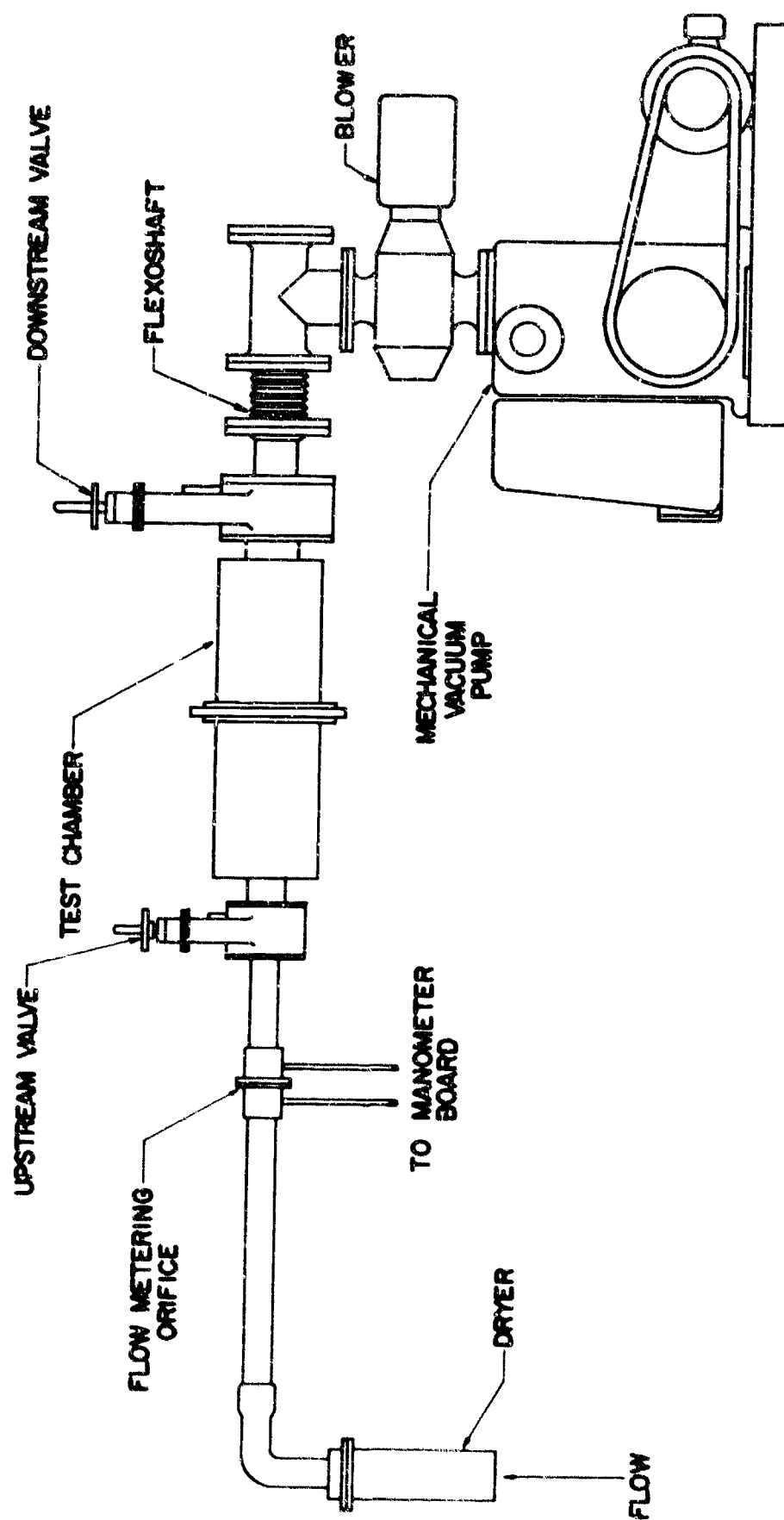


Figure 3. Sketch of Experimental Facility

one 1/2 inch O.D., the other 1/8 inch O.D., and a coiled capillary tube were employed. The mass flow through the system is found by measuring the pressure drop across each device when in use.

The upstream and downstream flanges were constructed so as to permit interchangeability. The corresponding ranges for each device are listed below:

capillary	$0.1 < Re^* < 8$
1/8" orifice	$2 < Re^* < 100$
1/2" orifice	$80 < Re^* < 2000$

All three flow metering devices were individually calibrated. The orifice plates, each constructed following A.S.M.E. specifications, were calibrated with water using the weigh-tank technique. Calibration accuracy was found to be within 1%. The coiled capillary tube was calibrated in place using a volumetric flow apparatus designed by S. McComas (5). This calibration likewise produced an accuracy of within 1%.

The manometer board was constructed with three U-tubes. The first was filled with oil, giving the pressure drop between the entrance of the dryer and the flow metering device. The other two were filled with oil and mercury respectively to measure the pressure drop across the flowmeter. The feed lines were fitted with valves to permit readings to be made with either oil or mercury. This allowed much larger ranges of Reynolds numbers to be covered with each device.

### 3. Upstream and Downstream Valves

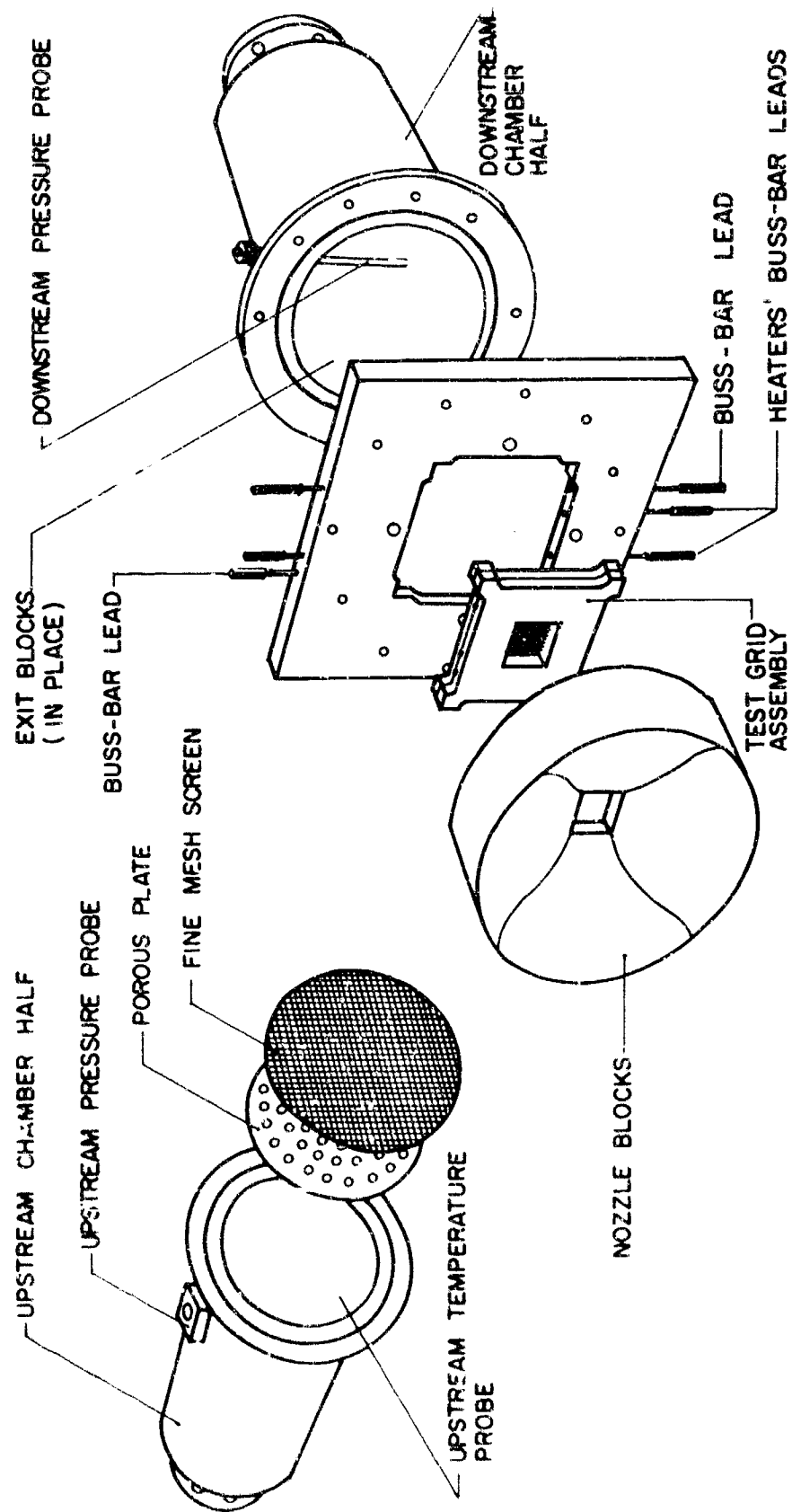
Two manually adjusted Temescal high-vacuum gate valves were installed in the system. Both have straight through connections designed for minimum resistance to flow and low outgassing characteristics. The upstream valve, two inches in inner diameter, was installed downstream of the flow metering device. This valve was used to throttle the flow and provided the main adjustment for upstream pressure. The downstream valve could be used to change the pressure ratio.

### 4. Test Chamber

The test chamber is shown in an exploded view in Figure 4. The chamber halves were cut from an 8-inch O.D. brass cylinder, fitted with flanges on each end. Each end was then bolted to the upstream and downstream valves respectively. In order to achieve uniform flow, a porous plate and fine mesh screen were encased in the upstream end. The central part of the porous plate was blanked off to further generate uniformity of flow. A mesh screen (60 wires per inch) was inserted 1-1/2 inches downstream to further break up the flow and reduce the scale of turbulence in the chamber.

The downstream half of the chamber was fitted with wooden exit blocks to provide a straight expansion angle of  $5^\circ$  leading to the pump. This prevented an abrupt expansion just aft of the test grid and provided a closer approximation to parachute performance.

An aluminum plate with a square cavity in the middle was located between the two chamber halves. The test section was mounted in this



### TEST CHAMBER ASSEMBLY DETAIL

Figure 4. Exploded View of Test Chamber

cavity (see Figure 5). The nozzle block was immediately upstream of the aluminum plate and attached to it (Figure 6). The nozzle block was machined from a linen phenolic rod, sanded and hand-polished in order to keep the roughness as low as possible. The primary concern in designing the nozzle blocks was to minimize the boundary layer thickness at the edge while preventing separation. The method of computing the nozzle profile was to compute the family of streamlines for the step geometry. To calculate the boundary layer thickness and to get some idea if separation occurs, an integral solution to the boundary layer equations was chosen. The method of Timman, given in (6), was used, as it allowed for the large pressure variations as appear in a nozzle. The optimum shape produced a boundary layer thickness of

$$\delta(\text{inches}) = 0.042/\sqrt{\text{Re}_1} \quad \text{Re} = \frac{\rho_1 U_1 d}{\mu_1}$$

at the nozzle block exit, with  $\rho_1$ ,  $U_1$ , and  $\mu_1$  also evaluated at the nozzle block exit.

A total pressure probe was installed upstream of the test grid in the stilling chamber, and a static pressure probe was inserted into the wall of the exit block, flush with the wall. The upstream operating pressure and temperature determined the sonic Reynolds number,  $\text{Re}^*$ . In addition, studies could be made of the pressure drop across the test grid with the two pressure probes.

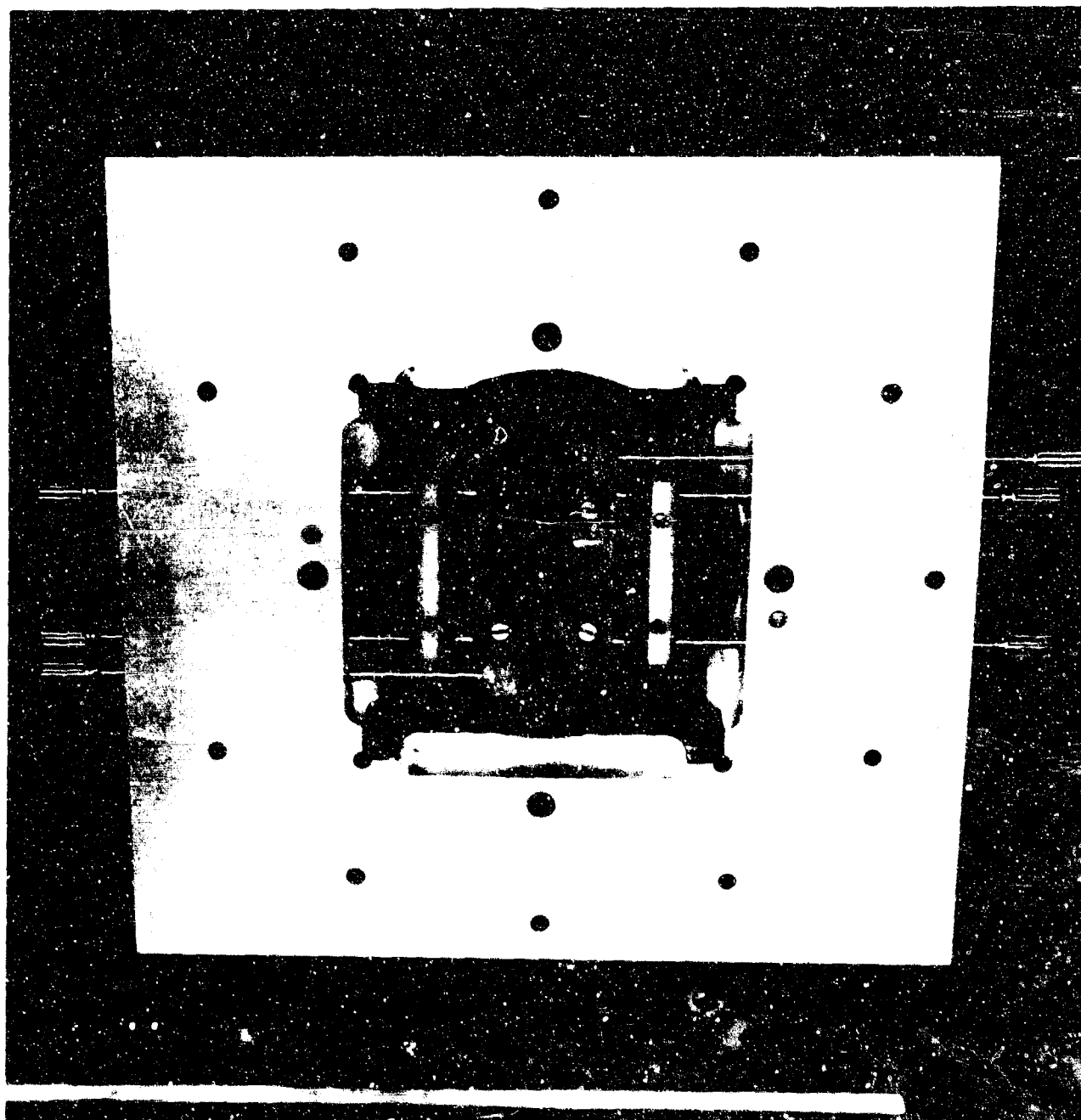


Figure 5. Aluminum Plate with Test Section and Housing Blocks

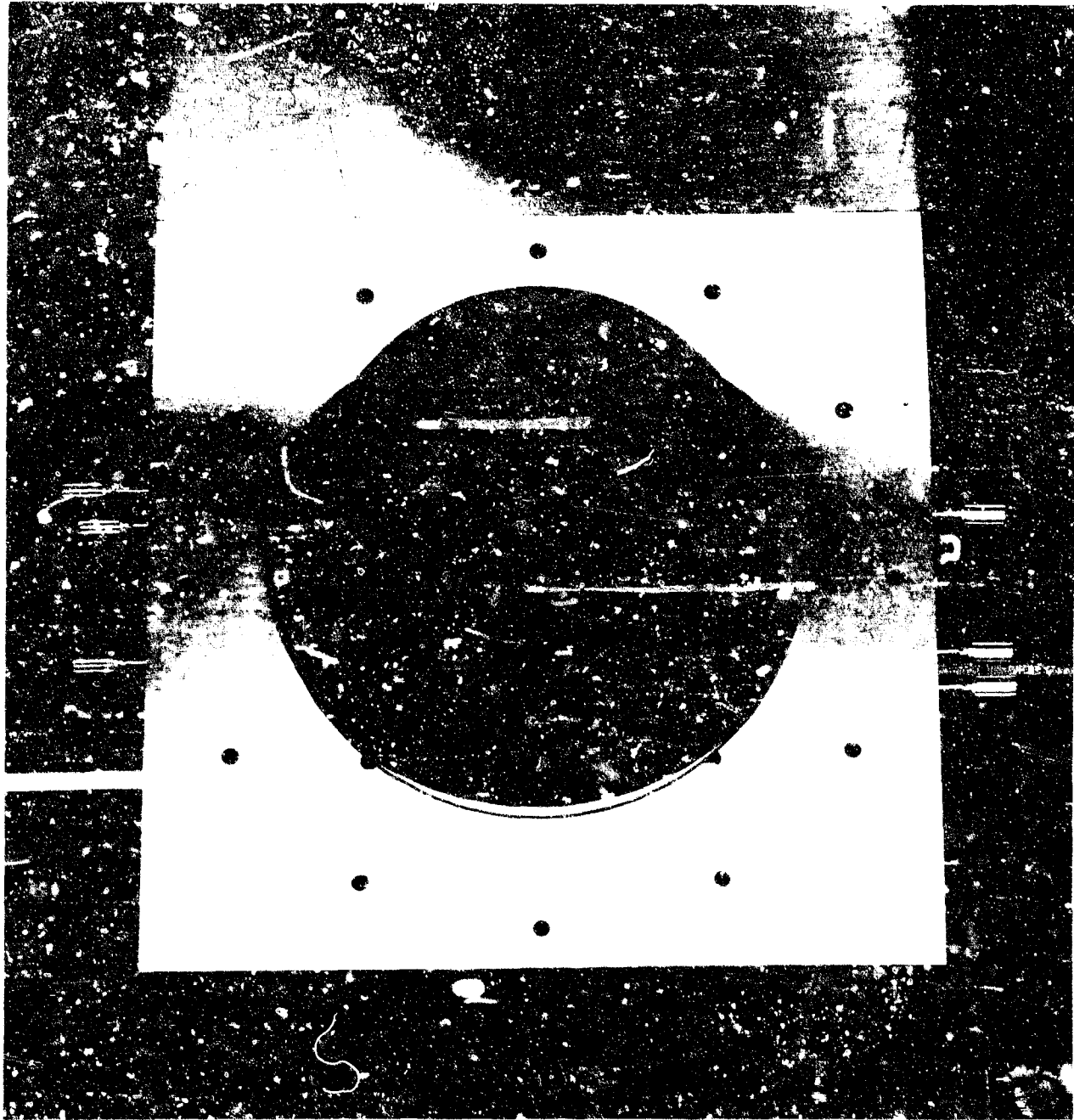


Figure 6. Aluminum Plate with Nozzle



After sealing all external joints of the test chamber with Glyptal, a moderately high-vacuum sealant, the system was leak-tested and found capable of maintaining a vacuum of less than 0.1 mm of mercury. This pressure level is one-twentieth of that corresponding to the lowest Reynolds number.

#### 5. Vacuum-Pump Combination

Two vacuum-pump combinations were selected in order to study the influence of the pressure ratio on the heat transfer coefficient. The first was the Dresser BSS 120-150 matched blower and pump. Its intake operating range is from  $10^{-2}$  mm of mercury to atmospheric pressure. The pump-blower combination maintains a constant pumping speed of 110 cu. ft. per minute for inlet pressures down to 1/2 mm of mercury, below which the pumping speed drops appreciably. This combination is the one which has been used mainly throughout these experiments.

The second vacuum-pump combination selected was the Dresser RS-260 DS-150 matched blower and pump. The pumping speed reaches a maximum of 240 cu. ft. per minute at an inlet pressure of 0.5 mm of mercury and decreases to 170 cu. ft. per minute at an inlet pressure of 100 mm of mercury; when the inlet pressure decreases below 0.1 mm of mercury, the pumping speed diminishes very fast to reach the value 0 at an inlet pressure of  $2 \times 10^{-3}$  mm of mercury. A Flexishaft coupling was installed just ahead of the pump (see Figure 3) to eliminate vibration in the wind tunnel.

## B. TEST SECTION

The test grid assembly is pictured in Figure 5. The housing blocks inserted in the square cavity of the aluminum plate were modeled of Scotchcast Brand Resin No. 250, capable of withstanding temperatures of 250°F—well above operating temperatures. The contact surface between plastic and metal was kept small to minimize conduction losses. The test screen shown in Figure 7 was sandwiched in and held by the two halves of each copper buss-bar, the under halves of which were screwed to the plastic housing, and the upper halves of which were screwed to the lower housing. Electrical guard heaters, consisting of narrow strips of very thin stainless steel (0.002"), were provided for each buss-bar. Heaters were isolated from the buss-bar through thin asbestos paper. Long copper leads were slid through the aluminum plate and screwed to the buss-bars and electric heaters respectively. Iron-constantan thermocouples were inserted one in each buss-bar. These thermocouples, together with the electric heaters, were used to control the temperature of the buss-bars such that heat conduction losses could be eliminated. The flow cross-section was  $3/4 \times 3/4$  inch. The square configuration was chosen to eliminate the extreme difficulty of producing uniform heat generation in a circular geometry.

The stainless steel test screens were cut from woven wire screens and silver-soldered to the copper pieces shown in Figure 7. The lateral sides of the wires were also silver-soldered to provide paths of uniform length and, with this, of the same electrical resistance; thus, uniform

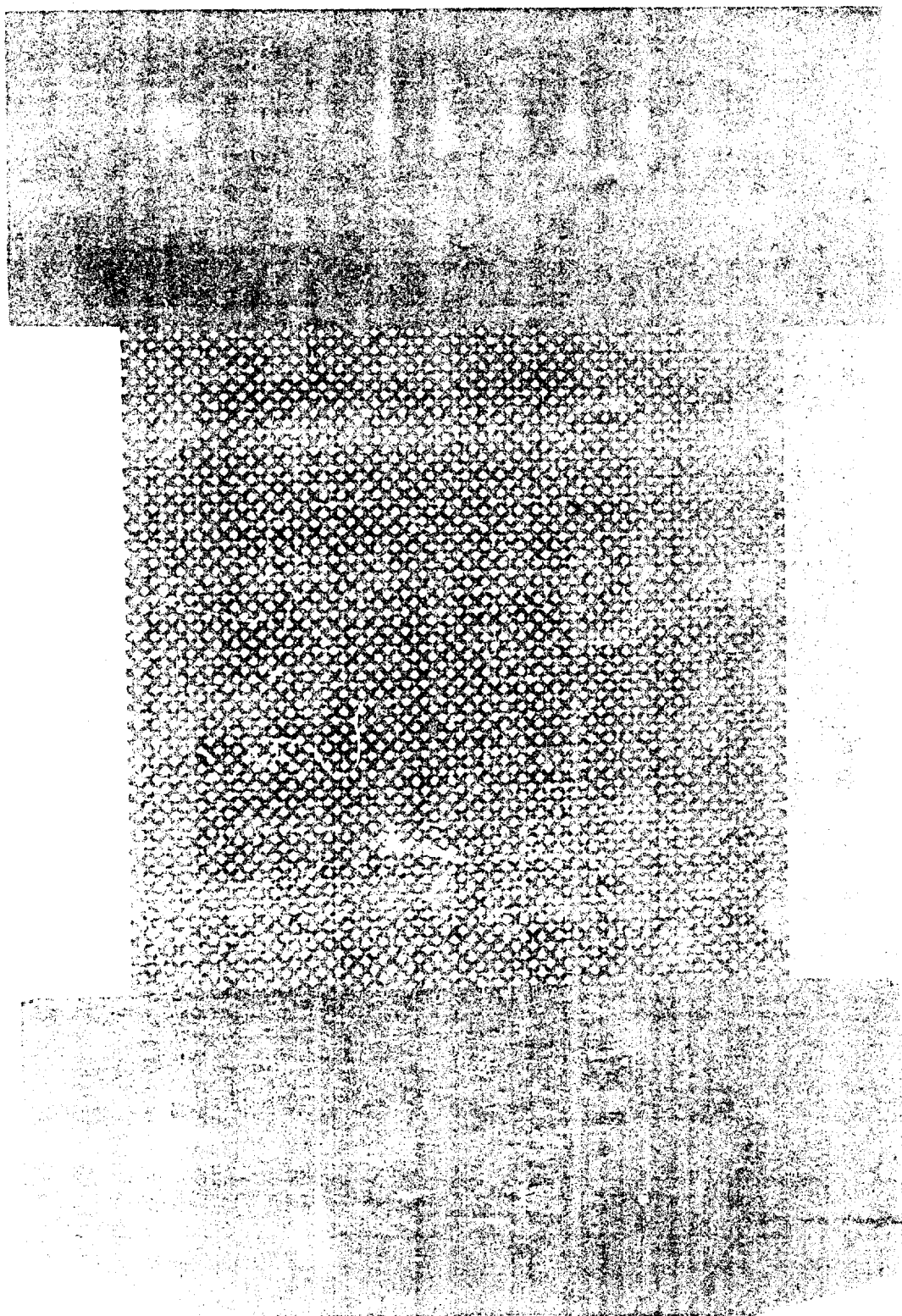


Figure 7. One Test Screen

Reproduced From  
Best Available Copy

heating could be obtained. Also, no difference in the electric potential should exist between the wires at any location where they touch.

Stainless steel was selected because of its relatively large resistivity, its high temperature resistance coefficient, and its strength, which allow smaller deformations under the influence of drag forces. The porosities were selected from those commercially available.

Three screens have been used, with the following properties:

	Screen 1	Screen 2	Screen 3
Diameter	0.0065"	0.007"	0.0055"
Wires/inch	70	60	80
Geometric Porosity	29.8%	33.9%	31.4%
Effective Porosity*	0.329	0.336	0.325

---

\* This is a different porosity used by Heinrich (7) for aerodynamic studies. The effective porosity  $C$  is defined as

$$C = \frac{U}{V}$$

with  $U$  the average velocity of the air through the screen and  $V$  a fictitious velocity, defined as

$$V = \frac{2\Delta p}{\rho}$$

where  $\Delta p$  is the pressure drop across the screen and  $\rho$  the density of the air downstream of the screen.

### C. INSTRUMENTATION

The instrumentation required for the test apparatus is of three types: temperature, pressure, and electrical.

Temperatures were sensed by 30 gauge iron-constantan thermocouples individually calibrated to an accuracy of  $\pm 0.1^{\circ}\text{F}$ . The calibration points were fitted with least square curves so that the temperature could be calculated on a computer. No significant error is initiated by this procedure. A list of vital thermocouple locations is given below:

1. Upstream bulk
2. Upper buss-bar
3. Lower buss-bar
4. Manometer board

The upstream total temperature was sensed by a probe positioned two inches upstream of the nozzle block and located in the geometric center of the stilling chamber.

The total upstream pressure was measured by an Alphatron Type 530 vacuum gauge made by NRC Equipment Corp. This instrument utilizes an ionization chamber with a radium source. It has seven decade scales ranging from 1000 to 0.001 mm of mercury. The accuracy is 2% of full scale reading.

All electrical measurements, including the thermocouple millivolt readings, were made with a Dymec 2010A digital acquisition system. This

system measures analog data including AC and DC voltages. Accuracy is 0.02% of full scale reading. The voltages measured were averaged over a period of one second. Current flow was found by employing precision shunts, each individually calibrated before use.

Owing to the inductive effects created by the woven mesh elements, DC power was used for all tests. The power was supplied by two six-volt storage batteries wired in parallel for the high Reynolds numbers and from a specially wired six-volt battery, giving three parallel-connected, two-volt cells, for the low Reynolds numbers.

In order to shield the test screen from electrical noises a metal screen was mounted far downstream of the test mesh. This screen, in conjunction with the metal screen used to increase the uniformity of the flow and the pipe system, formed a closed, electrically isolated volume.

### SECTION III

#### EXPERIMENTAL STUDIES

##### HEAT TRANSFER MEASUREMENTS

The goal of this experiment was to find the relation between the average heat transfer coefficient  $h$  and the sonic Reynolds number  $Re^*$ . The average heat transfer coefficient is given by

$$h = \frac{Q/A}{t_w - t_{aw}} \quad (3)$$

where  $Q$  is the heat input, given by the ohmic heating  $I^2R$ , with  $I$  being the intensity of the electrical current and the  $R$  the electrical resistance of the screen, and  $A$  the total area of the wires forming the test screen.

Originally the experimental apparatus was designed to work a slightly different way. The governing equations are given by a heat balance at the screen,

$$I^2R = hA(t_w - t_{aw}) \quad (4)$$

and by the well-known relation

$$R = R_0 [1 + \alpha(t_w - t_{w0})] \quad (5)$$

From the variables appearing in the equation,  $I$  and  $R$  are easy to measure, the first one by using a calibrated shunt and the second one with the help of a standard resistance. Further, with a previous calibration of the resistance  $R$  as a function of the temperature, a coul. be

found and, knowing  $R$  and  $\alpha$ ,  $t_w$  and  $t_{aw}$  could be read from the calibration curve. Once the temperature of the screen is known, the electrical guard heaters could be turned on and, with the help of a regulable resistance, the temperature of the buss-bar could be changed until the thermocouples inserted in them showed a temperature equal to  $t_w$ . In this way heat exchanges by conduction between the test mesh and the buss-bars could be avoided. Unfortunately, the indicated reference value  $R_0$  of the electrical resistance of the test screens sometimes changed with time. However, no changes in the resistance coefficient  $\alpha$  were observed. The absolute values of the changes of the resistance were within the order of magnitude of the changes due to a temperature variation between 0 and 50°F. After checking contact resistances, electrical noises, and ground problems, no reason has been found to explain the variations of the reference value of the resistance. Because of the inability to establish a relation between the electrical resistance of the test screen and its temperature, the experiment could not be carried out this way.

The observation that the changes of the reference value of the resistance  $R_0$  took place, not continuously, but rather stepwise at a certain moment, permitted us the development of a different way to perform the experiments. This method will be explained in the following paragraphs.

It can be shown that in the case that the reference value of the resistance  $R_0$  does not change during a running period, the resistance  $R$



should be a linear function of the square of the current intensity  $I^2$  (see Appendix I). If one measures the electrical resistance  $R$  for different intensities and finds corresponding points to be on a straight line, then one can extrapolate this line to the value  $I = 0$  and obtain a reference value  $R_0$  for each run. Appendix I shows that in this case the heat transfer coefficient  $h$  is given by

$$h = \frac{I^2 R R_0 \alpha}{A(R - R_0)} \quad \text{or} \quad h = \frac{R_0^2}{A} \tan \beta \quad (6)$$

( $\beta$  is the angle indicated in Figure 8).

As a general rule  $R$  was measured during each run for five or six values of the current (see Figure 8). The normal range of change of  $I$  was from 10 to 40 amps for the higher  $Re^*$  numbers and between 4 and 10 amps for the small  $Re^*$ . When the points so obtained did not plot on a straight line, it was assumed that the reference value of the resistance had changed during the running period, and the run was repeated. For the practical calculations the straight line was fitted using the criterion of the least square, with the aid of the computer. The largest error found in the accepted runs between any point and the fitted straight line was less than 0.07%. This is approximately equivalent to the change obtained in the resistance by increasing the temperature  $1^\circ F$ . Most of the relative errors were less than 0.01%.

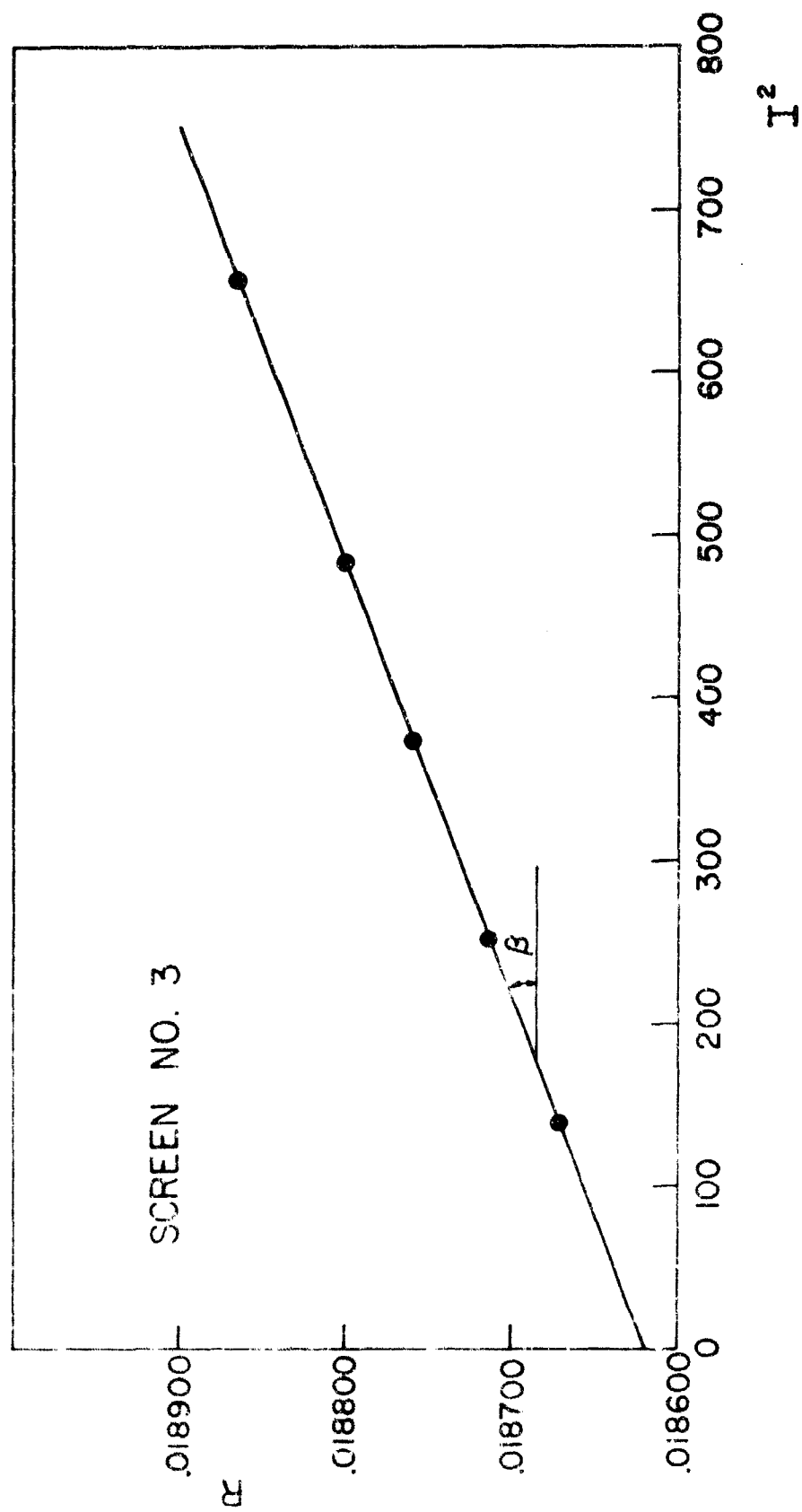


Figure 6. Example of Extrapolation Technique  
Used to Obtain  $R_0$

One disadvantage of this method is that it does not allow the use of the guard heaters, so that conduction losses could not be controlled. Therefore, an estimate of these losses was necessary (see Appendix II).

The sonic Reynolds number  $Re^*$  was changed by varying the upstream pressure (the air temperature in the room was almost constant; thus the sonic Reynolds number was a linear function of the upstream pressure only). The variation of the upstream pressure  $P_{up}$  was achieved by manipulating the upstream valve. When the pump-blower combination RSS-120-150 was used, the pressure ratio  $P_{up}/P_{down}$  could be maintained almost constant for all three screens--independent of the upstream pressure  $P_{up}$ --as shown in Figures 9, 10, and 11. The small oscillations shown may be due to small changes in the efficiency of the pump-compressor system with the input pressure and to the small errors in readings of the upstream and downstream pressures. When the pump-blower combination RS-260 DS-150 is used for low upstream pressures as shown in Figure 10, the efficiency of the pump-compressor system shows a much larger sensitivity to the inlet pressure, as described in Section II.A.5.

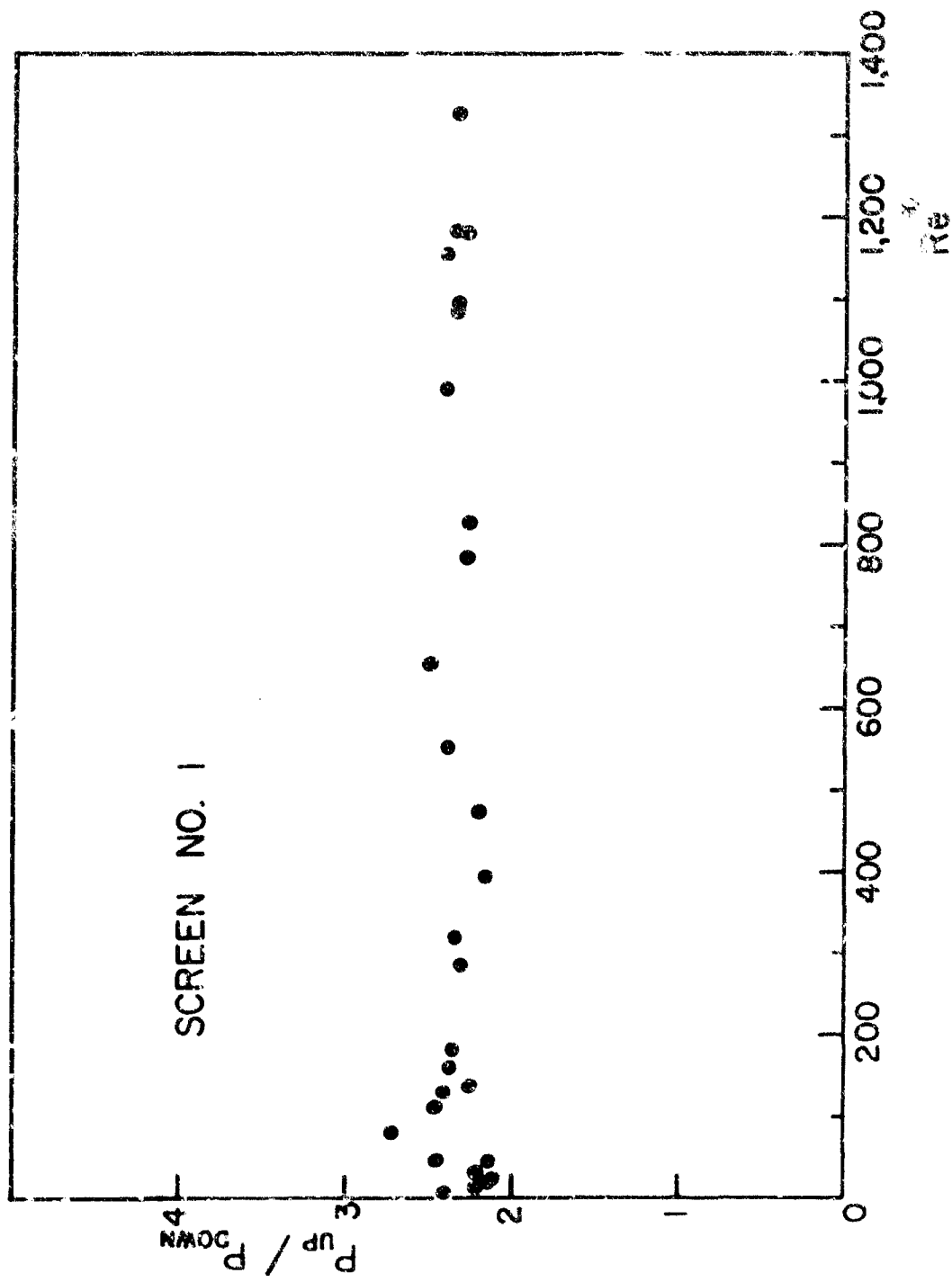


Figure 9.  $P_{up} / P_{down}$  Versus  $Re^*$  for Screen 1

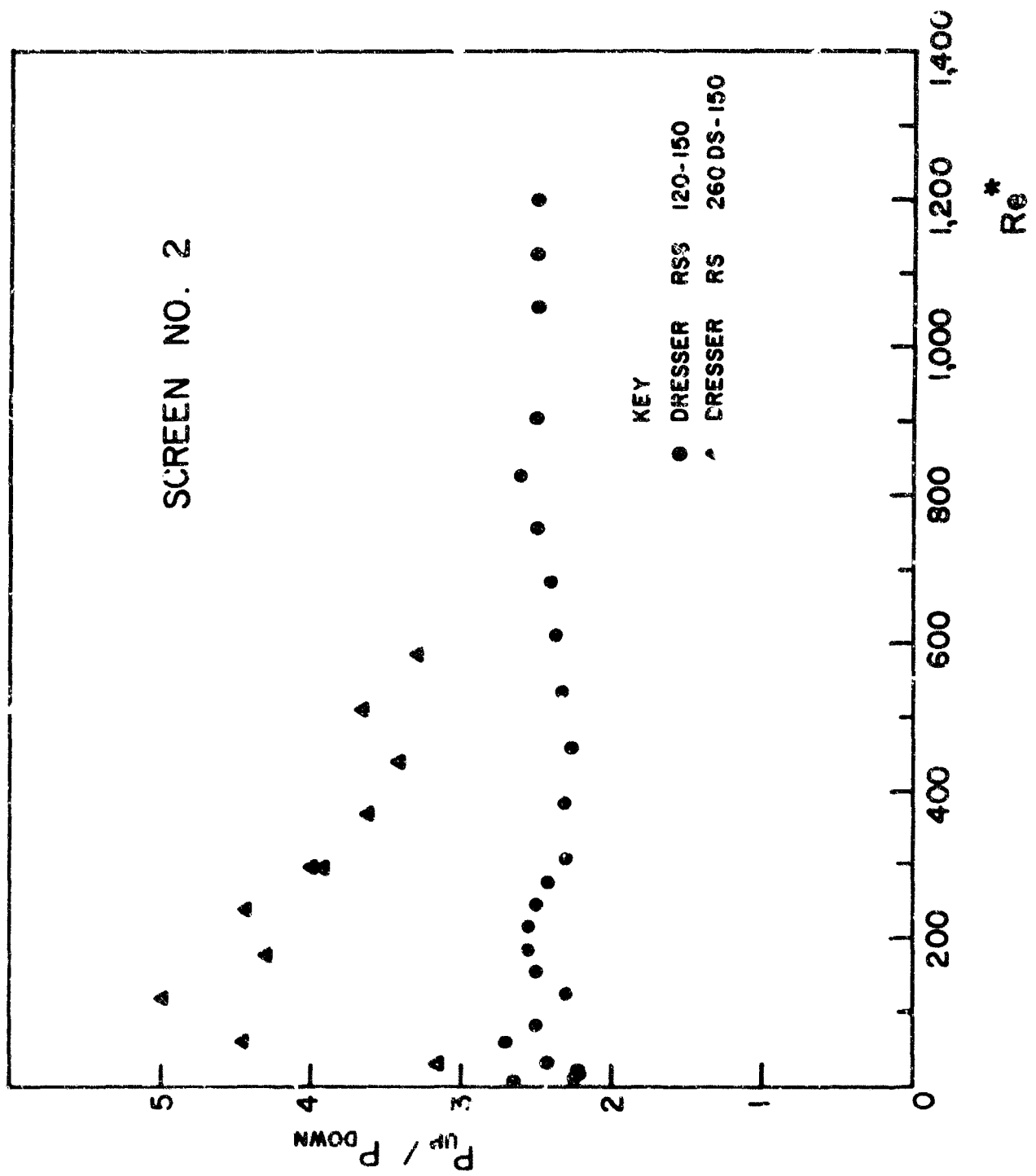


Figure 10.  $P_{up}/P_{down}$  Versus  $Re^*$  for Screen 2

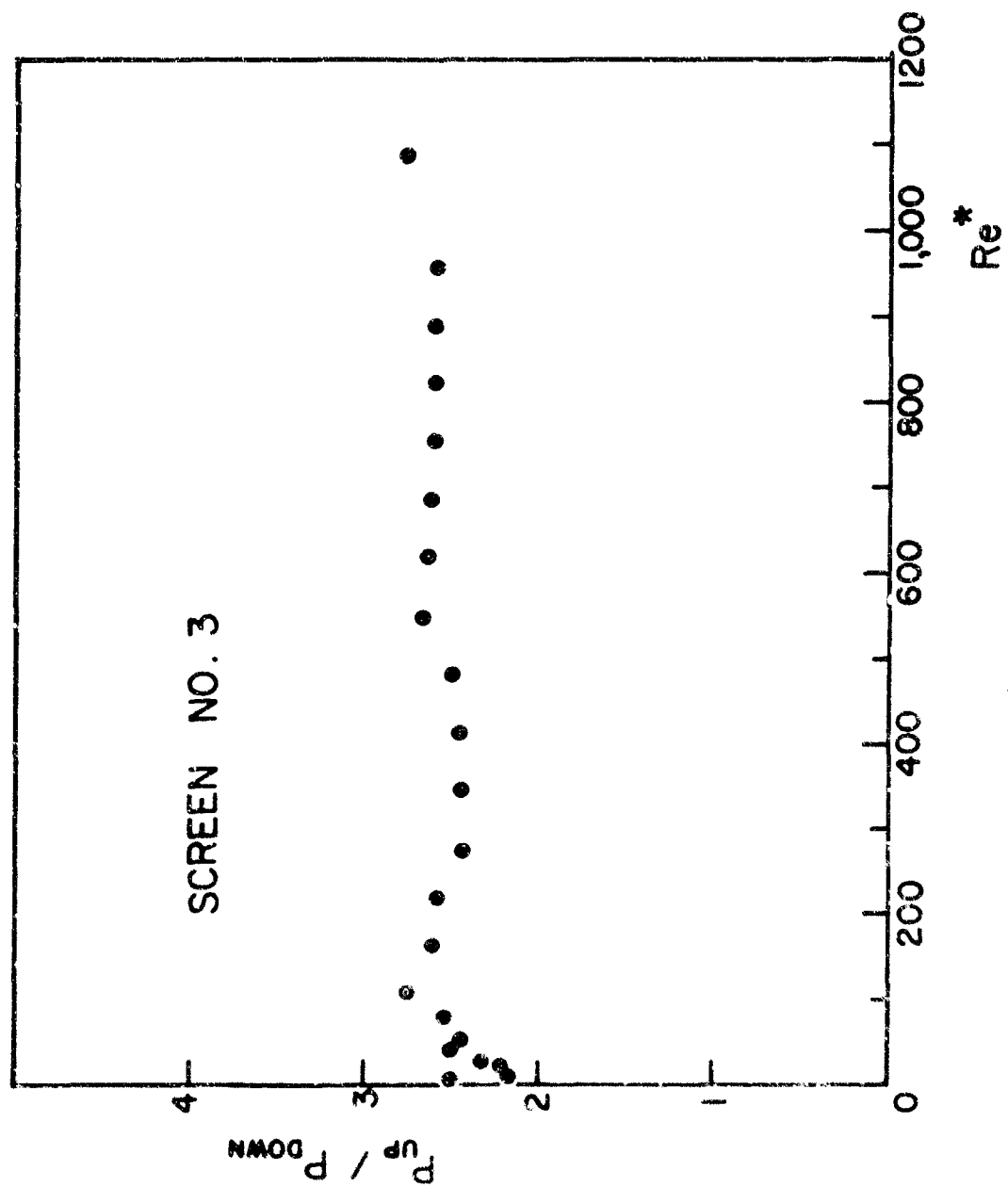


Figure 11.  $P_{up} / P_{down}$  Versus  $Re^*$  for Screen 3

## SECTION IV

### DISCUSSION OF RESULTS

The dimensionless Nusselt number,

$$Nu = \frac{hd}{k}, \quad (7)$$

based on the wire diameter, has been used instead of the dimension-dependent heat transfer coefficient. The results experimentally obtained are shown in Figures 12, 13, and 14, where the Nusselt number  $Nu$  has been plotted as a function of the sonic Reynolds number  $Re^*$ . In Figure 13 the values obtained by using the higher pressure ratio are also included. Although the influence of the pressure ratio  $P_{up}/P_{down}$  appears to be small, a tendency towards decreasing the dimensionless heat transfer coefficient with increasing pressure ratio can be observed. This phenomenon seems to be logical since a decrease of the pressure ratio, while holding the upstream pressure constant, indicates a lower downstream static pressure which should affect the local heat transfer coefficient in the manner noted.

No effects of the porosity  $Po$  on the average Nusselt number--within the relatively narrow range of porosities investigated--can be observed in Figures 12 through 14.

It is of interest to compare the measured Nusselt numbers for a screen with Nusselt numbers obtained for flow across a cylinder. Figure 15 is the result of such a comparison. The lines in the figure represent average Nusselt numbers as a function of upstream Reynolds number, with

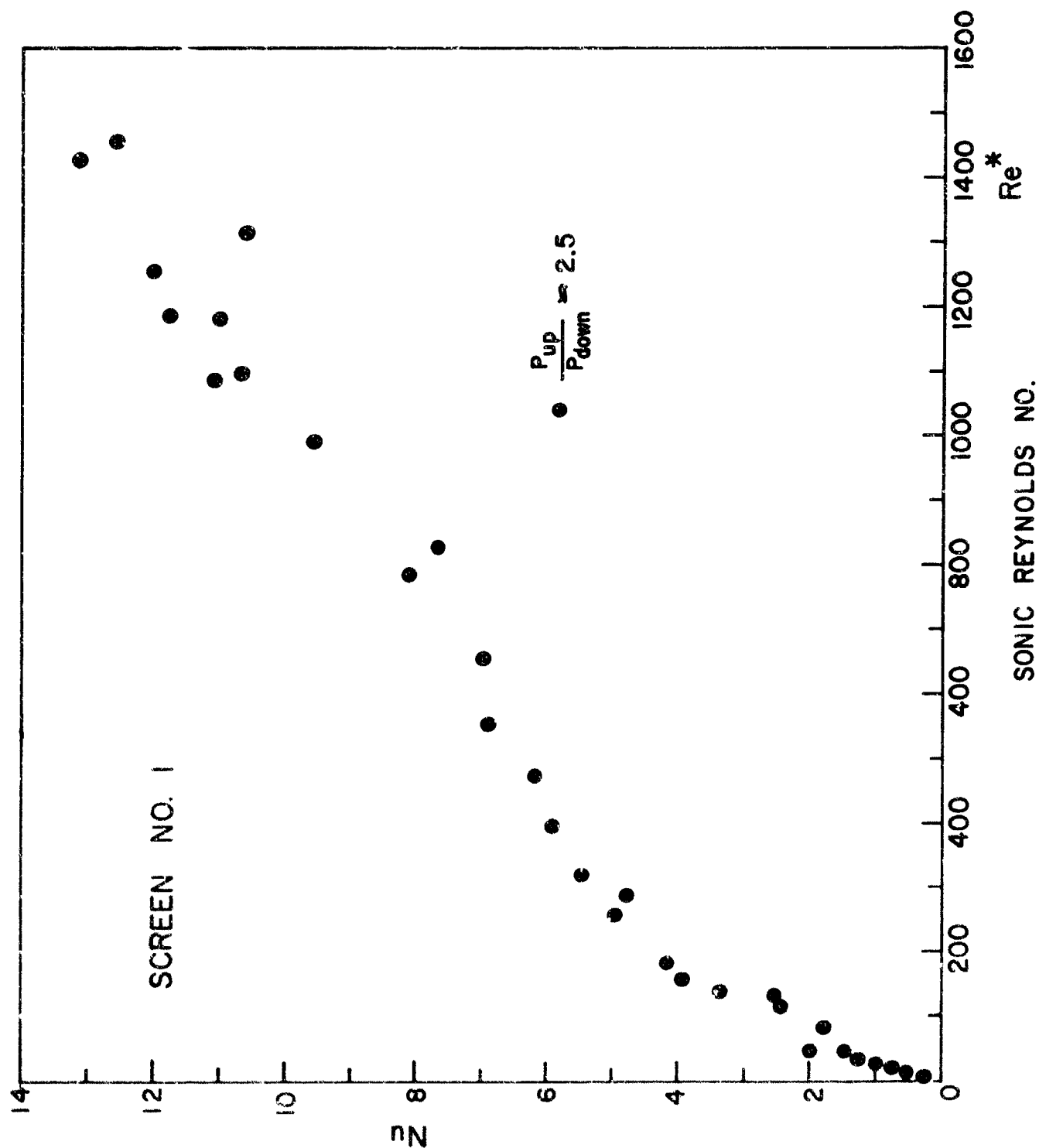


Figure 12. Nusselt Number Versus  $Re^*$  for Screen 1



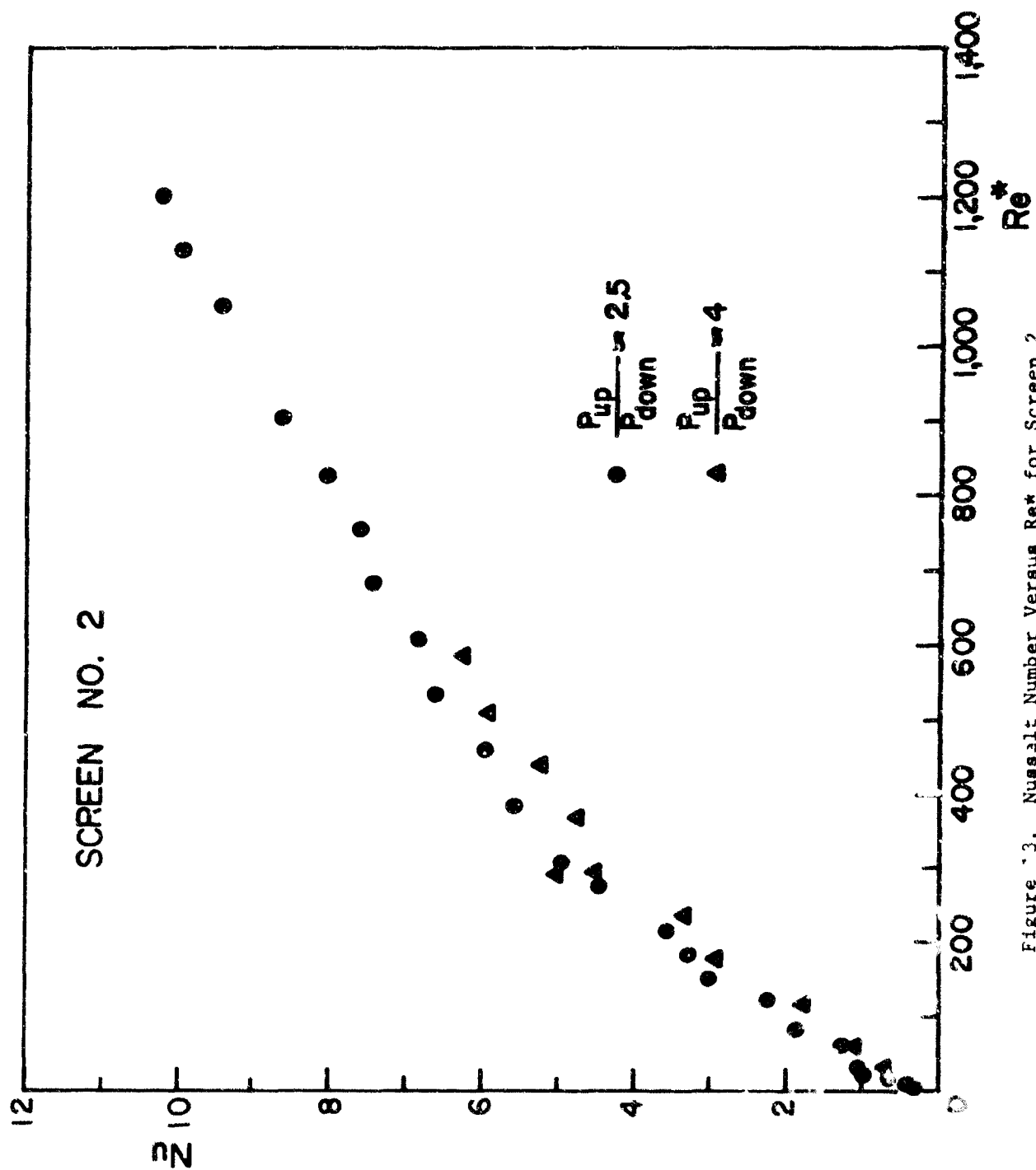


Figure 3. Nusselt Number Versus  $Re^*$  for Screen 2

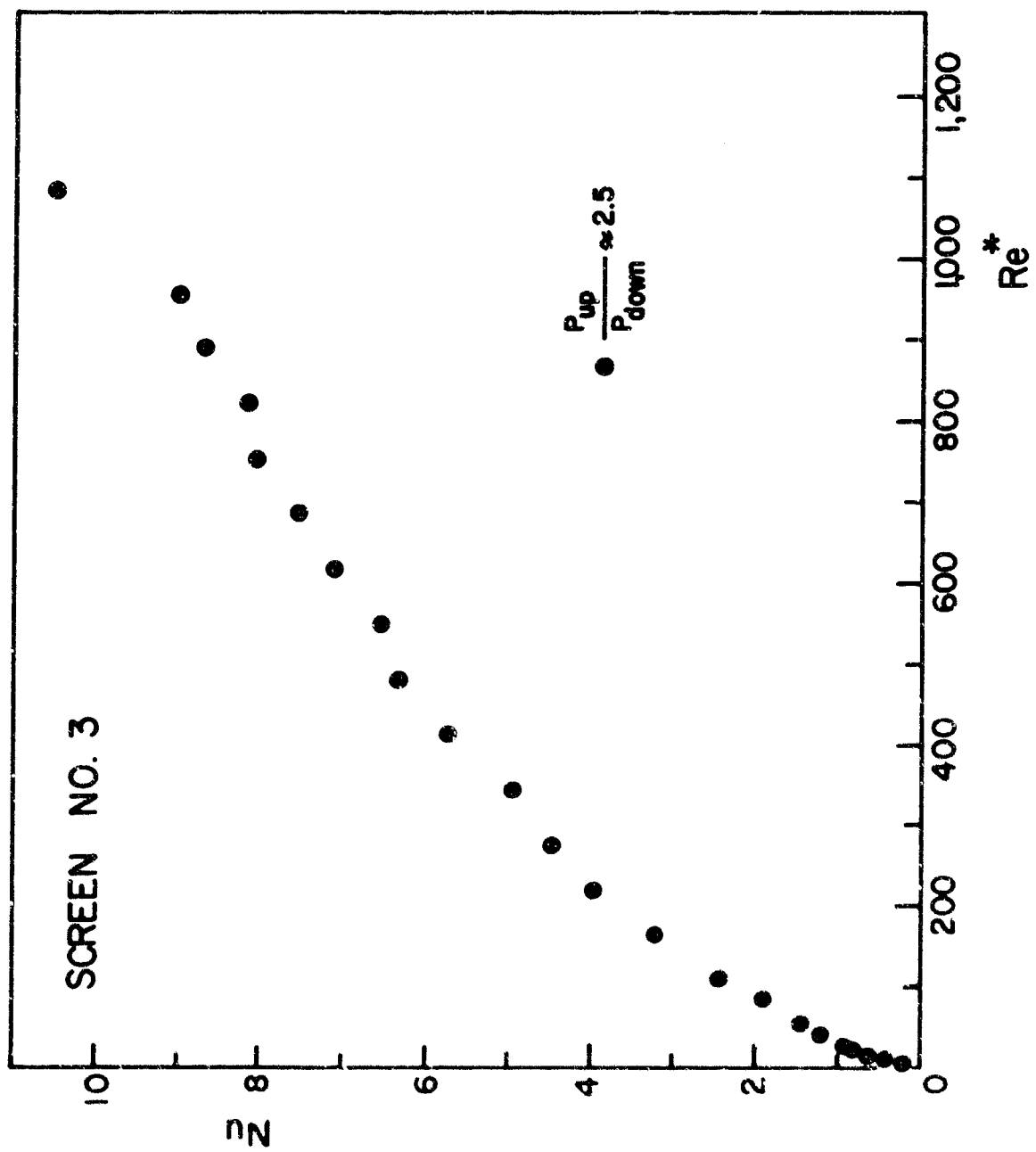


Figure 14. Nusselt Number Versus  $Re^*$  for Screen 3

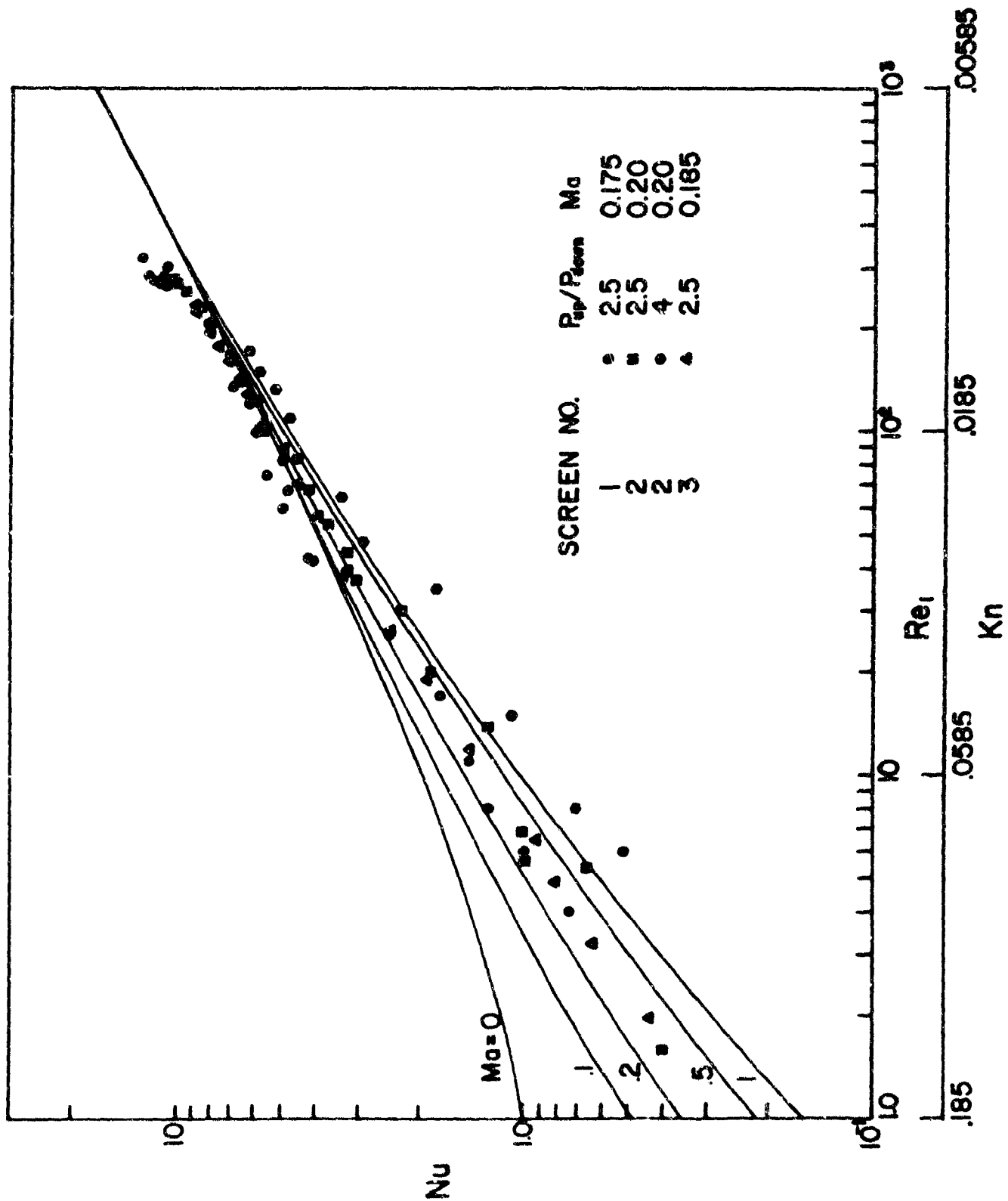


Figure 15. Comparison of Present Results with Results for a Cylinder

the upstream Mach number as a parameter. These Nusselt numbers have been taken from (8). The symbols in the figure refer to the results of our measurements. For this purpose the Reynolds number  $Re_1$ , based on flow conditions at the nozzle block exit and on the wire diameter, has been obtained from the sonic Reynolds number  $Re^*$ . The Mach number  $Ma_1$  was also calculated at this location. The Knudsen number<sup>\*</sup> calculated from the relation

$$Kn = \frac{Ma_1}{\sqrt{Re_1}} \quad (8)$$

is also indicated in Figure 15 as abscissa.

One should be careful in drawing conclusions from a quantitative comparison of the curves with the lines in this figure because of the difference in flow condition on a single cylinder and on a screen. For the same upstream flow condition, for instance, the maximum velocity outside the boundary layer on the cylinder is larger for the screen than for the single cylinder. Nevertheless a qualitative comparison certainly can be made and the figure indicates that rarefaction effects become important for Reynolds numbers lower than a value of order 100. This rarefaction effect also explains why the Nusselt numbers continuously decrease at about the same rate with decreasing Reynolds number, whereas in incompressible flow ( $Ma = 0$ ) the decrease of the Nusselt number diminishes

---

\* For plotting purposes in Figure 15, the Mach number  $Ma_1$  has been considered constant and equal to 0.185.

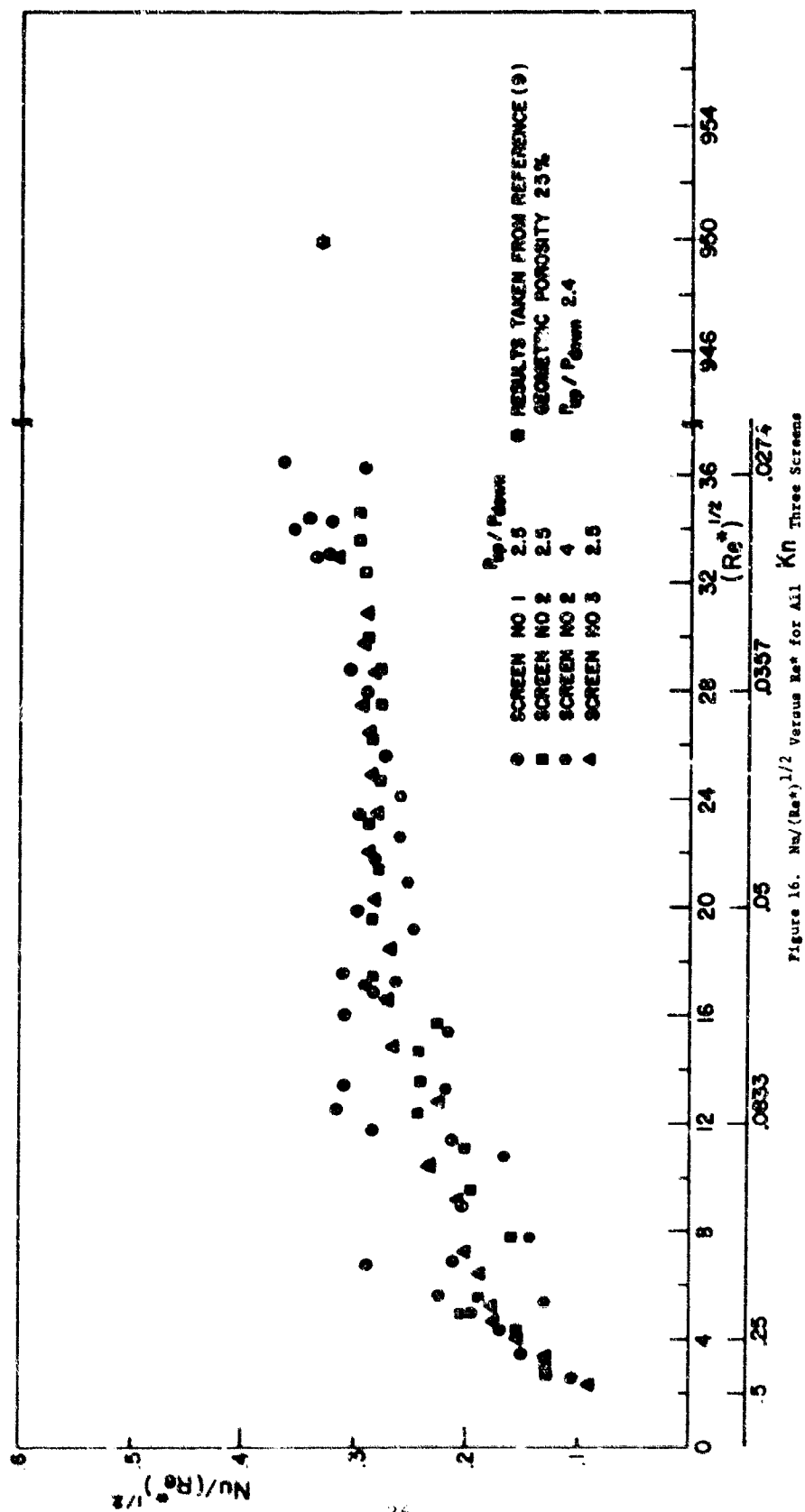
as the Reynolds number approaches the value 1. The figure shows that actually the agreement between the Nusselt numbers measured on the screens with values for a single cylinder is surprisingly good. Only at the highest Reynolds numbers investigated (beyond a value  $Re_1 \approx 250$ ) a sudden increase in Nusselt number is indicated which is not evident on the curves for the single cylinder.

In Figure 16 has been plotted the ratio  $Nu/(Re^*)^{1/2}$  versus  $(Re^*)^{1/2}$ . Here the value  $Nu/(Re^*)^{1/2}$  seems to be constant for  $Re^*$  larger than 400. In this figure are also included the integrated results reported in (9). In this study the local measurements were made on an enlarged woven mesh in which the individual fibers were one inch in diameter. The porosity and pressure ratio of the data in (9) closely match the present studies, while the sonic Reynolds number was considerably higher. The agreement between the integrated local values of (9) and the present average values is very good.

C. Scott derived the following expression describing the Nusselt number at the stagnation point of the wires in a screen from stagnation point boundary layer analysis (10):

$$\frac{Nu \left( \frac{L + D}{L} \right)}{Re^*} = 2 \times 0.496 \quad (9)$$

In Figure 17 this relation is compared with the measurements on the three screens. For sonic Reynolds numbers  $Re^*$  above a value of 400, the average



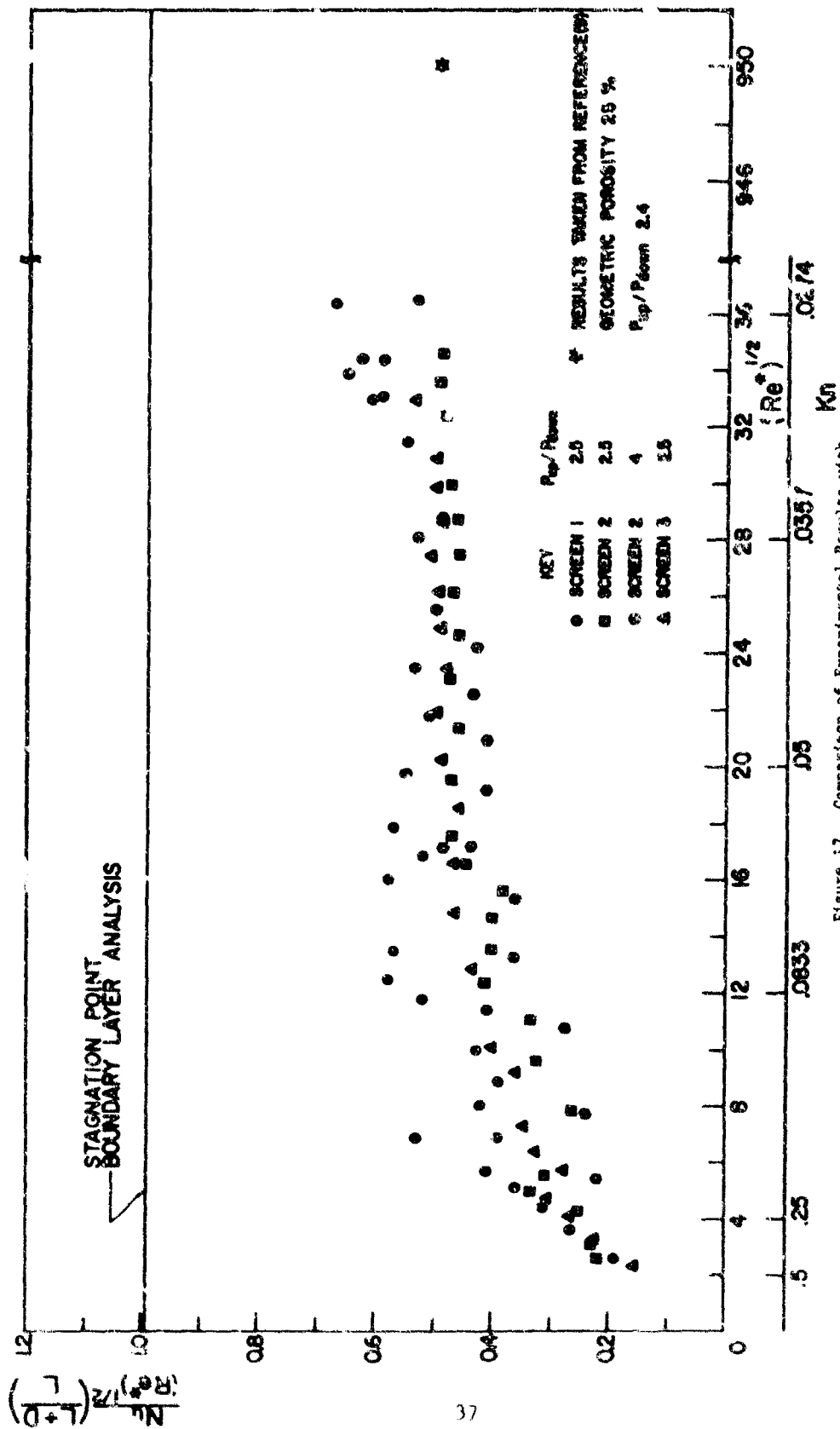


Figure 17 Comparison of Experimental Results with Theoretical Prediction

Nusselt number is by a factor of 2 lower than the one given in Eq. 9.

It can therefore be recommended to use the equation

$$\frac{Nu \left( \frac{L+d}{L} \right)}{Re^*} = 0.5 \quad (10)$$

for the calculation of average Nusselt numbers of screens with the porosity range investigated in our experiments. For sonic Reynolds numbers below 400, the average Nusselt numbers start dropping off with decreasing Reynolds number as a consequence of the rarefaction effects.

Figure 17 also contains the integrated values of (9). The agreement with the present values is also quite heartening.



## SECTION V

### CONCLUSIONS

Heat transfer experiments have been performed on three woven wire mesh screens simulating porous parachute cloth with porosities of 29.8, 31.4, and 33.9 percent. Average Nusselt numbers were measured as a function of sonic Reynolds number at a ratio 2.5 of the upstream total to the downstream static pressure. The results are presented in Figures 12 through 16. They indicate that rarefaction effects start to influence heat transfer when the Reynolds number  $Re^*$  based on sonic conditions decreases beyond the value of approximately 400 or for a corresponding value of the Knudsen number. Within the range of porosities which were investigated and the accuracy obtained, no effect of porosity on the average heat transfer coefficient could be established. The method of the ratio of the upstream total pressure to the downstream static pressure was checked on one of the screens and was found to be small for values between 2.5 and 4. The Nusselt numbers for screens are shown to have a behavior quite similar to the Nusselt number for a single cylinder in cross flow. The relation  $Nu(L + D)/Re^* = 0.5$  appears to be an acceptable representation of the average Nusselt numbers on screens for sonic Reynolds numbers above 400 for which rarefaction effects are not present.

## APPENDIX I

### DATA REDUCTION TECHNIQUE

Section III shows that the governing equations are

$$I^2 R = hA(t_w - t_{aw})$$

and

$$R = R_0[1 + \alpha(t_w - t_{w0})]$$

When the wind tunnel is running and  $I \neq 0$ , then  $t_{aw} = t_{w0}$  by the definition of the recovery temperature, so the equations can be rewritten

$$\frac{I^2 R}{A} = h \Delta t \quad (11)$$

$$\frac{R - R_0}{R_0 \alpha} = \Delta t \quad (12)$$

and, dividing Equation 11 by Equation 12,

$$\frac{I^2 R R_0 \alpha}{A(R - R_0)} = h \quad (13)$$

which is the formula used to calculate the heat transfer coefficient.

In order to show that the resistance  $R$  is a linear function of the square of the intensity of the current, Equation 13 is written

$$I^2 = \frac{hA(R - R_0)}{R_0^2 (1 + \alpha \Delta t)} \quad (14)$$

Now in our experiments the product  $\alpha \Delta t \ll 1$  (in general for the highest values of  $I$ ,  $\alpha \Delta t < 0.03$ ) so that this term can be neglected and Equation 14 gives

$$I^2 = \frac{hA}{R_0^2} (R - R_0) \quad (15)$$

which shows the desired relation between  $I^2$  and  $R$ .

## APPENDIX II

### ESTIMATE OF CONDUCTION LOSSES

Because conduction losses could not be eliminated, an estimate of them seems to be important.

The model used for the estimate of the heat conduction losses was a wire with uniform heat sources stretched between two walls, of prescribed temperature with the intensity of the heat source given by the ohmic heating. The solution is given in (11). The wire is cooled by convection. Its length is equal to the actual length of the wire measured from one buss-bar to the other across the soldered connection (Fig. 7). The average heat transfer coefficient measured in the experiments was used in the analysis. In Figure 18 are presented the results of the heat conduction correction for some key points.

An estimate of heat losses by radiation was also made assuming the shape factor for this exchange of radiant energy to be one. The heat transferred by radiation in this case will be larger than that corresponding to the actual situation. As a result we saw that the heat losses by radiation are of one order of magnitude smaller than the heat conduction losses, so they could be completely neglected.

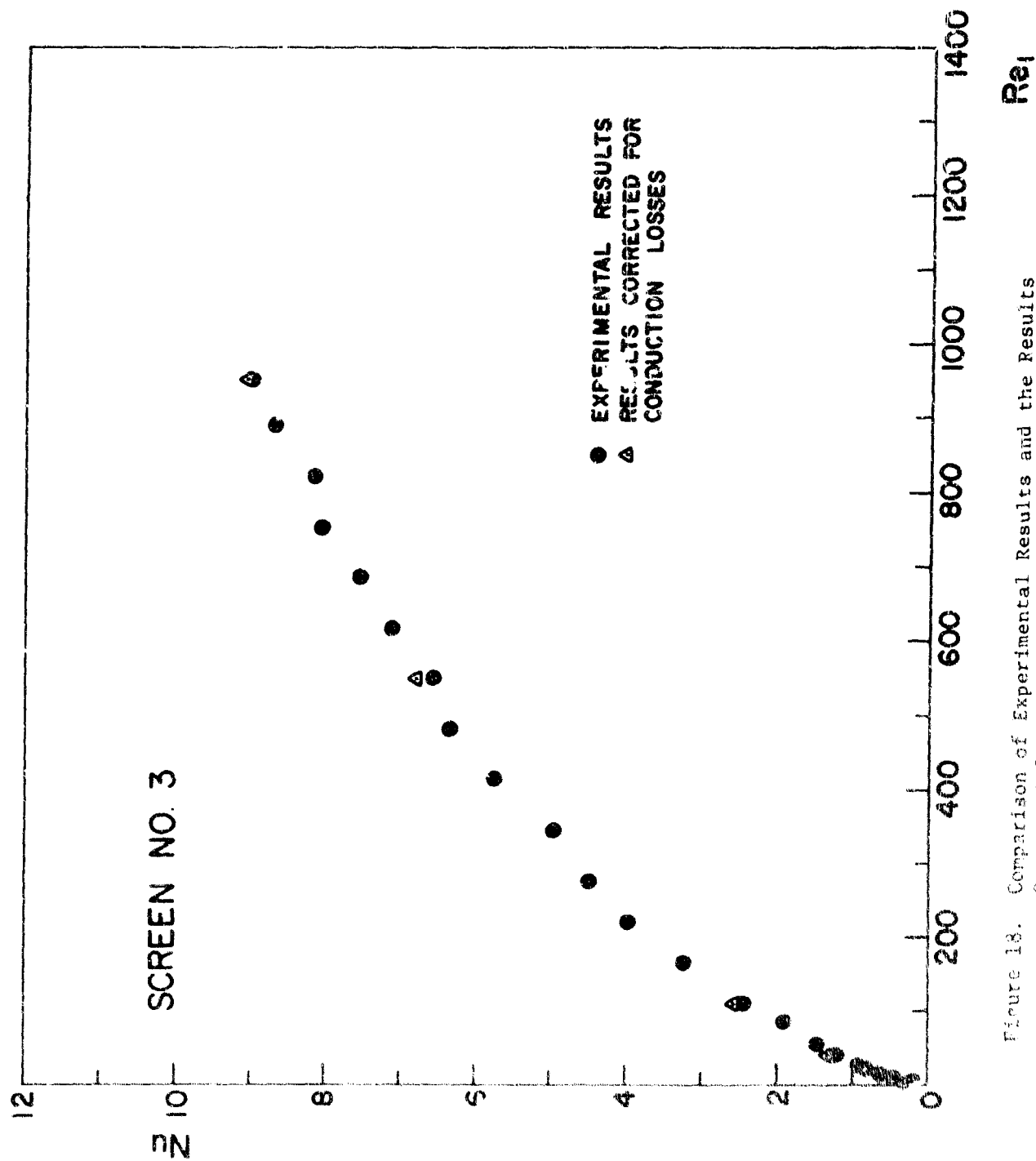


Figure 18. Comparison of Experimental Results and the Results Corrected for Estimated Heat Conduction Losses

# REFERENCES

1. Britzay, D., and Wiant, "Wire Cloth Structure for a Radiating Re-Entry Vehicle," AVCO-Everett Research Report 123, 1962.
2. Kyser, A. C., "The Rotornet: A High-Performance Hypersonic Deceleration for Planetary Entry," NASA CR-247, June 1965.
3. Koh, J. C. Y. and Hartnett, J. P., "Measured Pressure Distribution and Local Heat Transfer Rates for Flow over Concave Hemispheres," presented at the Semi-Annual Meeting of the American Rocket Society, Los Angeles, California, May 9-12, 1960.
4. Hansen, C. F., "Approximations for the Thermodynamic and Transport Properties of High-Temperature Air," NACA Technical Note 4150.
5. McComas, S. T., "Heat Transfer and Pressure Drop in Laminar Flow Through a Circular Tube Under Continuum and Rarefied Conditions," Ph.D. Thesis, University of Minnesota, 1964.
6. Rosenhead, L., Laminar Boundary Layers, Oxford University Press, 1963.
7. Heinrich, H. G., "The Effective Porosity of Parachute Cloth," Technical Report AFDDL-TR-65-182, University of Minnesota, 1966.
8. Baldwin, L. V., Sandberg, V. J., and Lawrence, J. L., "Heat Transfer from Transverse and Yawed Cylinders in Continuum, Slip, and Free Molecule Air Flows," Journal of Heat Transfer, May 1960.
9. Scott, C. J. and Ruiz-Urbina, H., "Experiments on the Distributions of Local Pressure and Heat Transfer on a Grid Simulating a Parachute Fabric," to be published in the Journal of Aircraft.
10. Scott, C. J., "The Prediction of Material Temperatures on Woven Retardation Devices," AFDDL-TR-67-170, University of Minnesota, 1967.
11. Eckert, E. R. G., and Drake, Heat and Mass Transfer, McGraw Hill, New York, 1959.

UNCLASSIFIED

Security Classification		DOCUMENT CONTROL DATA - R & D	
(Security classification of title, body of abstract and indexing annotation must be entered when the overall report is classified)			
1. ORIGINATING ACTIVITY (Corporate author) University of Minnesota Institute of Technology Mechanical Engineering Dept Minneapolis, Minnesota 55451		2a. REPORT SECURITY CLASSIFICATION Unclassified	
3. REPORT TITLE  Measurement of Average Heat Transfer Coefficients for a Mesh Simulating Porous Parachute Cloth		2b. GROUP N/A	
4. DESCRIPTIVE NOTES (Type of report and inclusive dates) Final Report - August 1966 - September 1967			
5. AUTHOR(S) (First name, middle initial, last name)  Scott, Charles J. et al			
6. REPORT DATE	7a. TOTAL NO. OF PAGES 11	7b. NO. OF REFS 11	
7c. CONTRACT OR GRANT NO. AF33615-67-C-1028		9a. ORIGINATOR'S REPORT NUMBER(S)	
b. PROJECT NO. 6065			
c. Task No. 606505		9b. OTHER REPORT NO(S) (Any other numbers that may be assigned this report) AFFDL-TR-67-171	
10. DISTRIBUTION STATEMENT This document is subject to special export controls and each transmittal to foreign governments or foreign nationals may be made only with prior approval of the AF Flight Dynamics Laboratory (FDFR) Wright-Patterson AFB, Ohio.			
11. SUPPLEMENTARY NOTES  N/A		12. SPONSORING MILITARY ACTIVITY AFDL (FDFR) Wright-Patterson AFB, Ohio	
13. ABSTRACT  Experimental heat transfer studies have been performed on three screens simulating a porous parachute. The average Nusselt number was measured as a function of the sonic Reynolds number. The range of the sonic Reynolds number extended from 5 to about 1400. Three different porosities and two different pressure ratios were used. Within the range of porosities and pressure ratios investigated, no significant effect of these parameters on the average heat transfer coefficient could be established. The Nusselt numbers for screens are shown to have a behavior quite similar to the Nusselt number for a single cylinder in cross flow. The relation $Nu(L+D)/Re^* = 5$ appears to be an acceptable representation of the average Nusselt numbers on screens for sonic Reynolds numbers above 400 for which rarefaction effects are not present.  The distribution of this Abstract is unlimited.			

DD FORM 1473

UNCLASSIFIED

Security Classification

